Microporous and Mesoporous Materials 132 (2010) 201–209

Contents lists available at ScienceDirect

Microporous and Mesoporous Materials

journal homepage: www.elsevier.com/locate/micromeso

Evaluation of the physical properties and photodegradation ability of titania nanocrystalline impregnated onto modified kaolin

Vipasiri Vimonses [a,b], Meng Nan Chong [a,b], Bo Jin [a,b,c,*]

[a] School of Chemical Engineering, The University of Adelaide, Adelaide, SA 5005, Australia
[b] School of Earth and Environmental Sciences, The University of Adelaide, Adelaide, SA 5005, Australia
[c] Australian Water Quality Centre, SA Water Corporation, Adelaide, SA 5000, Australia

ARTICLE INFO

Article history:
Received 2 December 2009
Received in revised form 11 February 2010
Accepted 22 February 2010
Available online 24 February 2010

Keywords:
TiO_2
Photocatalysis
Sol–gel
Kaolin
Thermal regeneration

ABSTRACT

In this study, a microporous layer photocatalyst of titania nanocrystallites heterocoagulated with structurally modified kaolin (TiO_2–K) was synthesised via a modified sol–gel method. Physical properties (particle size, morphology, stability and settleability) and photodegradation capacity of the TiO_2–K catalyst subject to its synthesis, regeneration and use for water treatment were studied. The modified kaolin, as a support for the titania nanocrystallites had a delaminated sandwich silica structure that minimises chemical intercalation within the nanocomposite structure. Microscopic examination revealed that the TiO_2 nanocrystallites were uniformly deposited on the kaolin external surface, resulting in a high degree of photon activation. Compared to the commercial TiO_2 P25, the TiO_2–K demonstrated a superior photocatalytic degradation capacity to remove an anionic Congo red dye. Its removal efficiency and photo-reaction performance were improved when the TiO_2–K was regenerated by a thermal treatment. The TiO_2–K particles can be easily separated from the water system for further reuse. This unique nanocomposite photocatalyst shows promising technical advantages for a continuous industrial process of water treatment.

1. Introduction

The multi-faceted properties and photocatalytic performance of titanium dioxide (TiO_2) for water purifications have received an increasing interest in recent decades owing to its high photostability, non-toxicity and cost effectiveness [1]. Many successes in TiO_2-assisted photodegradation toward recalcitrant organic contaminants in water, including different complexes endocrine disrupting compounds and dyes has been well-documented [2–4]. In reality, however, such heterogeneous photocatalysis processes for water purification utilising commercial TiO_2 are still facing a number of constraints that annihilate its feasibility for an industrial application.

Since the main photo-induced charged separation occurs on the surface of the photocatalysts, a larger specific area would promote a higher photocatalytic reaction rate. Herrmann [5] suggested that adsorption is a pre-dominant step in ensuring rapid photocatalytic surface reaction on the water contaminants. Owing to the large surface area to volume ratio, nanosized photocatalysts (i.e. Degussa P25) present a significant physical advantage that compromises the organic adsorption. These nanosized TiO_2 photocatalysts can lead to a latent difficulty for a downstream process to separate and recover the TiO_2 particles before reaching the consumer-end. Such ultra-fine particle separation usually incurs high operation and capital costs, and thus has seriously impeded the large scale applications of TiO_2 photocatalysts for an industrial treatment process.

Immobilisation of the nanosized TiO_2 photocatalysts can avoid the problem associated with the post downstream process required to separate the TiO_2 catalysts. Such a deposition method is usually technically-subjective, and requires significant experimental efforts to optimise between the surface areas to volume ratio of the supported-photocatalysts with its photoactivity. The exploitation of various titania-supported-photocatalysts to achieve desirable physicochemical properties, photoactivity and stability for water treatment has received a great attention [6]. Deposition of TiO_2 thin films onto a larger catalyst support, such as ferromagnetic cores or silica materials considerably improved both the particle recovery and adsorptive capacity [7]. Different layer silicate materials such as clay minerals were investigated as a possible supporting platform for the TiO_2 nanocrystals [8,9]. A few studies have explored the possibility of clays-supported TiO_2 nanocrystals, with frequent emphasis on the natural montmorillonite subclass. So far, a little attention has been paid how the physicochemical

* Corresponding author. Address: School of Chemical Engineering, The University of Adelaide, North Terrace Campus, Adelaide, SA 5005, Australia. Tel.: +61 8 8303 7056; fax: +61 8 8303 6222.
E-mail address: bo.jin@adelaide.edu.au (B. Jin).

1387-1811/$ - see front matter © 2010 Elsevier Inc. All rights reserved.
doi:10.1016/j.micromeso.2010.02.021

properties and photoactivity of the TiO_2 nanocrystals could be varied during the photocatalytic process, especially if the catalysts are repeatedly recovered and reused in a water purification system.

In this study, we synthesized a thin-layer TiO_2 nanocrystalline impregnated onto physiochemically modified kaolin as the immobiliser platform. Natural kaolin, $Al_2Si_2O_5(OH)_4$, is a phyllosilicate (sheet silicates) mineral with a tetrahedral silica sheet alternating with an octahedral alumina sheet. The ideas of exploiting kaolin is owing to its relatively low isomorphous substitution within its lattice structure, that limits the molecular interaction in water system, in which the clay structure can be possibly altered as found in montmorillonite. Such an ordered structure of kaolin, however, can restrict its functional active site to the plane and edge of kaolin particles. To improve the physical surface properties of kaolin as the catalyst platform, we investigated for the first time a series of pre-treatment methods of the kaolin prior to the sol–gel deposition of TiO_2 thin film, including acid dissolution, alkaline treatment and thermal activation. That was followed by controlled heterocoagulation of the TiO_2 sol with the treated kaolin particles, as previously reported by this team [8]. The resultant physicochemical properties of the TiO_2-impregnated kaolin (TiO_2–K) nanocomposites were characterised using X-ray diffractionometry (XRD), Brunauer–Emmett–Teller (BET), and electroscopic techniques of scanning electron microscopy (SEM) and transmission electron microscopy (TEM). Such techniques were also used to unveil the variation in physicochemical properties during different thermal regeneration cycles. Photoactivity of the TiO_2–K catalyst was evaluated against the degradation of anionic Congo red dye as a model surrogate compound. The settleability of the photocatalyst particles were also analysed using Kynch's hindered settling conditions, in terms of the single photocatalyst particle terminal settling velocity.

2. Materials and methods

2.1. Materials

Physicochemical properties of kaolin may be varied, depending upon the geographic source of origin. Natural white dry-milled kaolin obtained from Unimin, Australia was used in this study. The kaolin consisted of SiO_2 (48.7%), Al_2O_3 (34.6%), TiO_2 (1.3%), Fe_2O_3 (0.9%) and other trace compositions of K_2O, CaO, MgO and Na_2O. The details of the physical and chemical properties of the kaolin materials were reported in our previous work [10]. Commercial TiO_2 P25 (Degussa, Germany) was used as received for comparison study. The Degussa P25 has a surface area of $50 \pm 5\ m^2\ g^{-1}$ and composes of 80% anatase and 20% rutile with elementary particle size of 25–85 nm, respectively.

Titanium (IV) butoxide (tetrabutyl orthotitanate AR grade $\geq$ 97% gravimetric, Sigma–Aldrich), absolute ethanol (AR grade, Labserv Pronalys, Australia), and sodium pyrophosphate (AR grade, BDH VWR, England) were used as received. Congo red (CR) ($C_{32}H_{22}N_6Na_2O_6S_2$, Labchem Ajax Finechem, Australia), sulphuric acid (AR grade, 98 wt%, BDH VWR, England), nitric acid (AR grade, 69 wt%, BDH VWR, England), sodium hydroxide (AR grade, BDH VWR, England) were prepared using double-deionised water with 18.2 M-ΩM, resistivity.

2.2. Pre-treatment on natural kaolin clay

Natural kaolin was first pre-treated, in order to purify and augment the surface availability prior to the subsequent heterocoagulation process with TiO_2 sol. A series of acid–alkaline-thermal treatment was performed to alter the surface properties of the clay. Kaolin suspension (ca. $20\ g\ L^{-1}$) was magnetically suspended in a 20 cm high jar that fills with deionised water for particle size screening. At a certain stirring extent, the suspension was allowed for settling within 0.5 h. Supernatant from the jar containing particles with a size range <10 μm was decanted and filtered. The filtrate cake was then resuspended in 1 M sulphuric acid solution with continuous stirring up to 10 h before being filtered and washed repeatedly with deionised water. Following this, the kaolin particles were treated by 2 M sodium hydroxide at pH 10 for 0.5 h. The final kaolin filtrate cake was washed and dried at 70 °C for 4 h before firing at 750 °C for 1 h.

2.3. Synthesis of TiO_2–kaolin Catalysts

Deposition of TiO_2 thin film onto surface-augmented kaolin was prepared according to our previously reported method [9]. Twenty-five millilitre titanium (IV) butoxide was vigorously mixed with 30 mL of absolute ethanol for 0.5 h. The mixture was then acid catalysed via backdrop into a controlled-molar nitric acid solution. After the acid catalysed reaction a transparent homogeneous TiO_2 sol was then attained under continuous stirring for 0.5 h. Following this, the homogeneous TiO_2 sol was carefully heterocoagulated with the treated kaolin (ca. 10% w/v) via slow addition of the sol into the vigorously-stirred kaolin suspension. The stirring flask was kept at 37 °C in a water bath. Heterocoagulated TiO_2–kaolin was continually stirred for 4 h, before aging for 14–16 h at room temperature. The aged nanocomposites were then filtered and washed repeatedly with deionised water to remove any excess chemical impurities. Then, the nanocomposites were dried at 70 ± 2 °C for 2–4 h to remove any surface-bound water molecules before calcination at 600 °C at a heat ramping rate of 4–5 °C min^{-1} for 3 h. The final product of TiO_2–K particles was readily used as photocatalysts for the following experiments.

2.4. Characterisation of kaolin and TiO_2–K catalysts

The following analytical methods were conducted to characterise both the raw kaolin and TiO_2–K particles. This information is useful to gain insight into the physical, chemical and photochemical characteristics of the TiO_2–K particles using surface-augmented kaolin as a support platform.

Differential temperature analysis coupled with thermogravimetric analyser (DTA–TG) (TA Instruments) was performed on the raw kaolin to obtain the weight loss of kaolin as a function of temperature. During the analysis, the raw kaolin sample was heat-treated from room temperature to 1200 °C at a ramping rate of 10 °C min^{-1} under highly nitrogenised condition to avoid any possible oxidation.

Particle size of pre-treated kaolin was then measured using a static light scattering laser diffraction particle sizer instrument (Malvern Mastersizer 2000), covering the detection range from 0.02 to 2000 microns. The kaolin particles were first dispersed in sodium pyrophosphate solution, with constant agitation and sonication until a stable dispersion was attained. The particle size distribution of the pre-treated kaolin particles from the particle size screening are as shown in Fig. 1.

Morphological and surface characteristics of the resultant TiO_2–K particles were analysed using SEM (Philips XL30 SEM) at an accelerating voltage of 10 kV. Thin platinum coating was applied on the particle sample prior to analysis. TEM was also performed using Philips CM-100 TEM at an accelerating voltage of 100 kV. Before the analysis, the TiO_2–K particles were minimally suspended in ethanol solution (ca. 0.01% w/v), followed by ultrasonic dispersion and subsequent immobilisation on the copper measurement grids of 2 mm diameter.

BET specific surface area and pore size measurements on the resultant nanocomposites were performed using a micrometrics

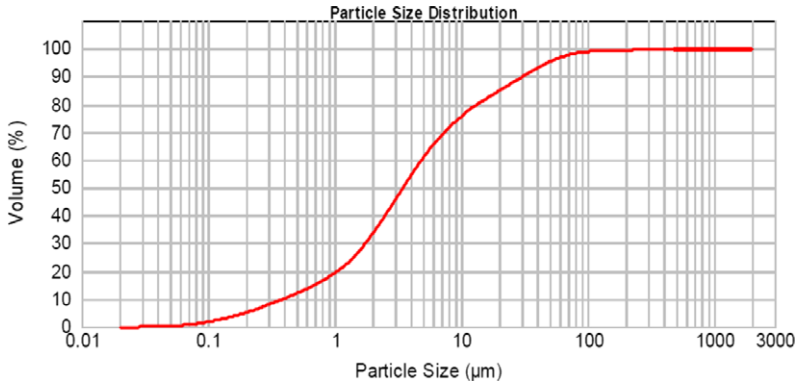

Fig. 1. The particle size distribution of natural kaolin ($d_{0.1}$ = 0.396 µm, $d_{0.5}$ = 3.471 µm and $d_{0.9}$ = 30.558 µm).

gas adsorption analyser (Gemini Type 2375) at 77 ± 0.5 K in liquid nitrogen. Prior to the surface analysis, the sample vessels loaded with ca. 0.5–1.0 g were vacuum treated overnight at 105 °C and evacuation pressure of 50 mTorr. Nitrogen adsorption isotherms of the samples were then analysed for the specific surface area using the BET equation.

The material composition analyses of the samples were measured using X-ray Fluorescence (XRF) technique. One gram of the oven dried sample (105 °C) was accurately weighed with 4 g of 12–22 lithium borate flux. The mixtures were heated to 1050 °C in a Pt/Au crucible for 20 min to completely dissolve the sample then poured into a 32 mm Pt/Au mould heated to a similar temperature. The melt was cooled rapidly over a compressed air stream and the resulting glass disks were analysed on a PANalytical Axios Advanced wavelength dispersive XRF system using the in-house Silicates calibration program.

XRD measurements were performed using a Philips PW Diffractometer (Cu X-rays λ = 1.54 Å) over the range of 5–75° 2θ for all the samples. Samples were spiked with 10 wt% of zinc oxide before the diffractionometric analysis to facilitate the determination of amorphous phase TiO_2 to the amount of TiO_2 nanocrystals formed. The average crystallite diameter of the TiO_2 nanocrystals, D_{hkl}, was obtained using the Debye–Scherrer equation ($D_{hkl} = k\alpha/\beta \cos\theta$), where β is the line broadening, k is the crystalline shape with Warren's correction value for instrumental broadening of 0.89, and α and θ are the radiation wavelength and Bragg angle, respectively. A standard for the line broadening width based on a single anatase crystal of TiO_2 was used for calibration.

Optical absorption characteristic of the resultant TiO_2–K composites was measured using a UV–vis diffuse-reflectance spectroscopy. The diffuse-reflectance spectra were measured using a Varian Cary 5000 UV–vis spectrophotometer between the wavelengths of 250 to 600 nm.

2.5. Photoactivity assessment of TiO_2–kaolin catalysts

Photoactivity of the resultant TiO_2–K was probed using CR as a standard photo-oxidation rate. Aqueous solution of 57.4 µmol L^{-1} CR was photochemically reacted with TiO_2–K in a preliminary experiment. An 11 W UV-C light (Davis Ultraviolet, Australia) was positioned centrally to a magnetically-stirred beaker that contained the reaction solution. The linear attenuation of the UV intensity at the reaction solution surface was determined to be 300 µW cm^{-2} using a radiometer. Prior to the photochemical reaction, the TiO_2–K was remained in dark homogenisation for 0.5 h allowed to ensure constant dispersion and mixing. Sampling was conducted every 1 h, and the supernatant was obtained for calorimetric measurement via centrifugation at 5000 rpm for 10 min. Single maximum wavelength of 496.5 nm was used with a path cell length of 1 cm in a UV–vis spectrophotometer for analysing CR concentration. The CR concentrations were measured in triplicate and were evaluated as the average photo-oxidation rate.

3. Results and discussions

3.1. Surface augmentation of kaolin clay as nanocrystal support

Raw kaolin was initially subjected to acid treatment to purify the clay through dissolving the undesired chemical impurities that may be present naturally or during the manufacturing process. The presence of a high level of impurities in the raw kaolin might severely affect the interlayer pore space and thus, the total effective surface area. Komadel and Madejová [11] stated that the acidification of clay mineral under a controlled acid condition might also induce partial dissolution of other undesired elements (i.e. Fe and Mg) within the clay structure. Such acid attack is known to preferentially occur at the octahedral alumina sheet, while the tetrahedral sheet (i.e. SiO_4 and SiO_3OH) remain largely intact [12].

In this instance, reaction time for the kaolin acidification remains a crucial factor for effective surface augmentation while maintaining a stable alumina structure for immobilising the TiO_2 nanocrystals. We found that at an acidification time shorter than 10 h, the leaching rate of both the Fe and Mg cations to the Al cation was suppressed from the clay structure (data not shown). Such a retention time was found to be relatively shorter than those previously reported by Steudel et al. [12]. The partial dissolution of kaolin during the acidification process, however, induces delamination of kaolin structure, in which the remaining tetrahedral sheets are connected to the residual octahedral sheet. The acidification of the kaolin resulted in formation of micropores within the kaolin structure, and consequently an increase in both the specific surface area and porosity. The BET adsorption isotherms calculation indicated that the specific surface area of the acidified kaolin increased from 20.3 to 26.1 m^2g^{-1}. The acidification of the kaolin can also be proven from the apparent color change of the kaolin from yellowish to white, as a result of the low level of chemical impurities present.

To counterbalance the net positive surface of the acidified kaolin, a subsequent alkalization treatment step was carried out to shift the surface charge to be slightly negative. The extent of such alkalization treatment is important, in order to promote the latter heterocoagulation between the positively charged TiO_2 sol and the kaolin particles. Such an alkalization treatment, however, is quite complicated to implement across kaolin particles of different point of zero charge (PZC); kaolin (ca. 4–4.7) and its edges (ca. 6–7) [13,14]. In our study, we adjusted the kaolin suspension with so-

dium hydroxide to pH 10 to ensure the conversion of surface charge. In contrast to acidification, tetrahedral silica compounds are more dissoluble in alkaline media than the Al, Fe and Mg cations. Jozefaciuk et al. [15] reported that alkalization is beneficial in purifying kaolin of the most irregular amorphous mineral structures.

Thermoanalytical measurement of the kaolin was eventually performed to understand the stability of the kaolin structure against elevated temperature gradient (Fig. 2). From the DTA–TG plots of the acidified–alkalized treated kaolin, the initial peak of weight loss was found to correspond to the removal of surface-bounded water and other attached foreign molecules on the kaolin surface. This dehydration stage was manifested by the onset of endothermic process at 153 °C. The second weight loss peak that appears at endothermic temperature of 503 °C was related to the water dehydroxylation between each silicate pair sheets within the skeleton kaolin structure. The following exothermic peak at 985 °C was an indicative of the maximum applicable firing temperature before the collapse of kaolin structure. Thus, in order to maintain the skeleton kaolin structure, the treated kaolin particles heated up to 750 °C at a heating rate of 10 °C min^{-1} to prevent any undesirable adverse structural change.

Changes in the surface morphology of the fired kaolin structure were subsequently compared with the raw kaolin via SEM imaging. Fig. 3a shows the morphological surface of the raw kaolin particles, where the scattering of hexagonal flakes were piled up on top of one another along with consistent distribution of micropores. The SEM image presented in Fig. 3b shows that the surface structure of the treated kaolin particles was changed to rather flat surface with a low porosity. Such surface augmentation, as a result of the series of acidification–alkalization-thermal treatment, provides an increased surface area for ease of light accessibility and TiO_2 sol deposition. Eventual BET measurements revealed that the treated kaolin particles had a significantly enlarged specific surface area of 31.3 $m^2 g^{-1}$ compared with the raw kaolin particles of 20.3 $m^2 g^{-1}$.

3.2. Physicochemical properties of TiO_2–kaolin

It is well known that the photo-oxidation capacity of a photocatalyst can be strongly influenced by its physicochemical properties, which include size and morphology, crystalline phase, specific surface area and porosity. In this section, we primarily reported the physicochemical properties of the TiO_2–K particles.

Since the prepared TiO_2–K particles consist of layers of TiO_2 nanocrystals with kaolin, the thickness of the nanocrystal growth was carefully monitored using TEM. A consistent TiO_2 nanocrystal layer with an average size distribution of 7–9 nm was observed (Fig. 4a). Such layered TiO_2 nanocrystals can significantly alter the surface morphology of the core kaolin particles. It can be ob-

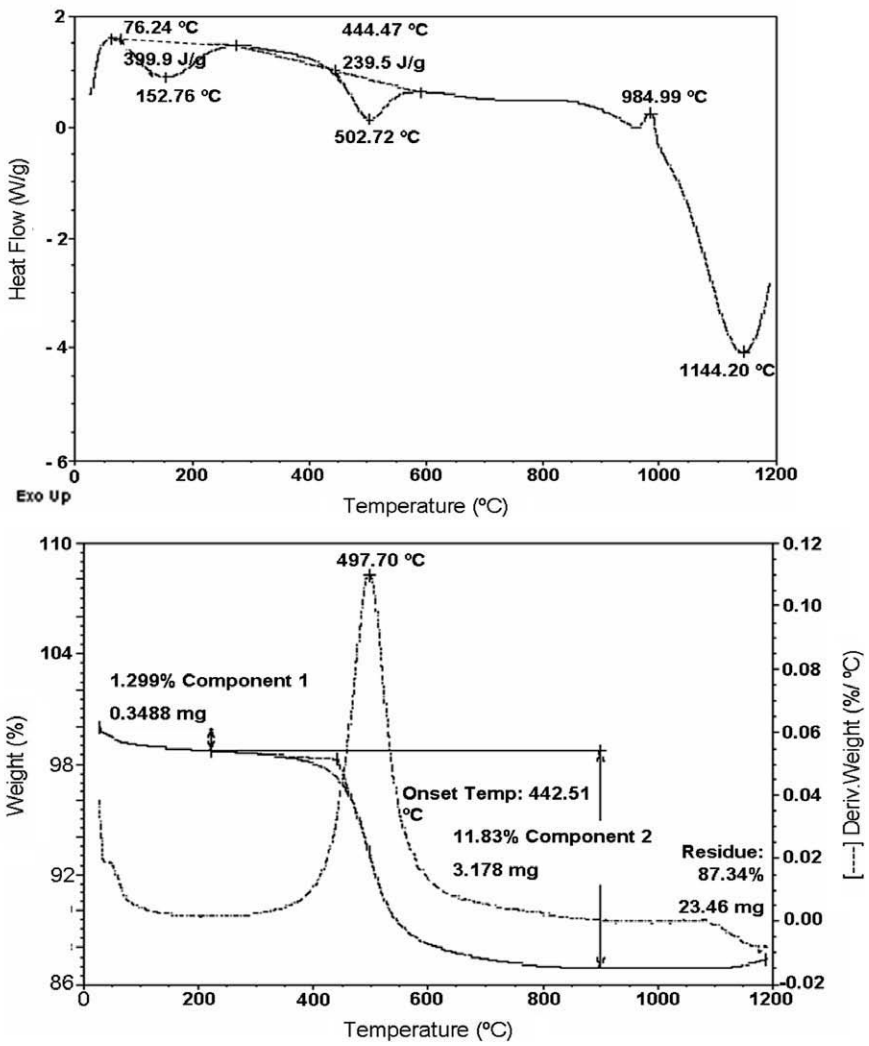

Fig. 2. Differential thermal analysis (DTA – heat flow against temperature profile) and thermogravimetric (TG – weight loss against temperature profile) of natural kaolin.

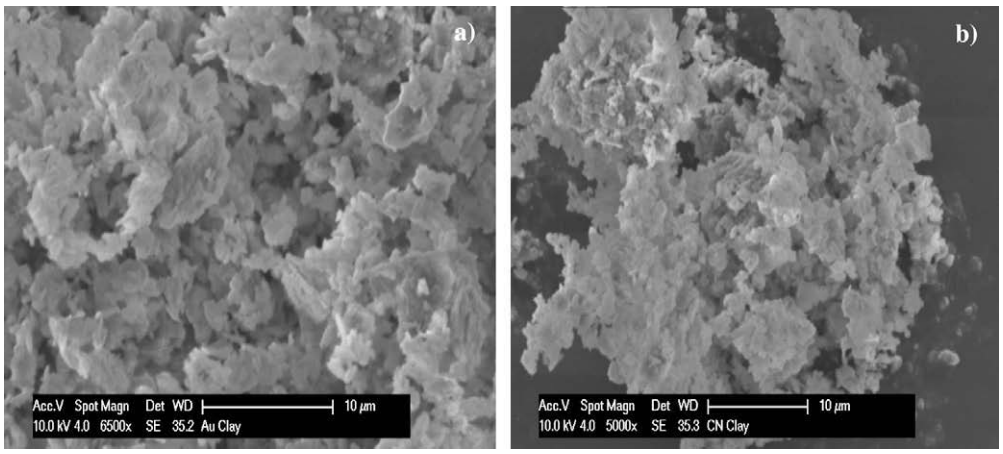

Fig. 3. SEM images of kaolin (a) without pre-treatment and (b) with treatment.

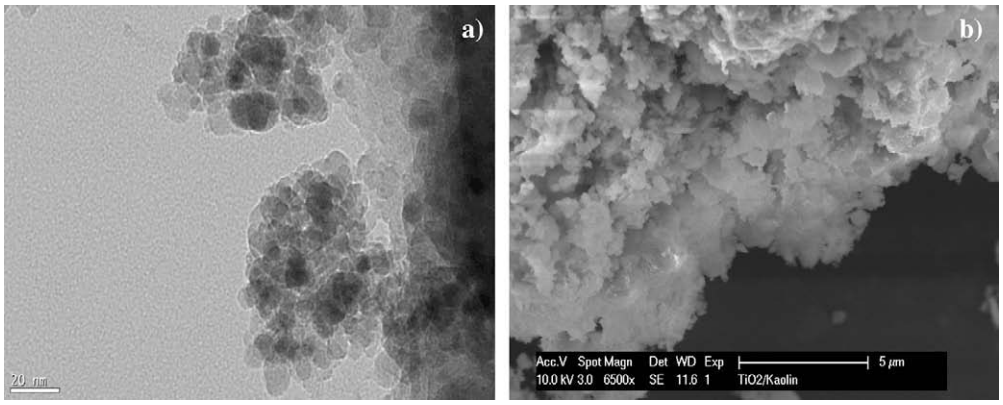

Fig. 4. Electron microscopy images of TiO_2–K (a) TEM and (b) SEM.

served that a highly porous structure (Fig. 4b) was attained after the controlled deposition of TiO_2 nanocrystals, as this is relative to the flat sheet prototype of pre-treated kaolin particles. Presence of such deposited TiO_2 nanocrystals remarkably increased the specific surface area of the kaolin. This was evidenced from the specific surface area and average pore size of the nanocomposites, as determined using nitrogen adsorption measurements. These results show that the specific surface area increased from 31.3 to 57.6 $m^2\ g^{-1}$, and the average pore diameter was estimated to be 8.3 nm, suggesting the prominent existence of microporous TiO_2 structure on the surface of core kaolin particle.

XRF analysis showed that the TiO_2–K consisted of TiO_2 (18.67%), SiO_2 (42.47%), Al_2O_3 (35.61%) and Fe_2O_3 (0.25%). XRD measurements on the TiO_2–K particles revealed that the crystalline TiO_2 constitutes by anatase TiO_2 phase alone. Fig. 5 suggests that the layered TiO_2 is made up of anatase structure as evidenced by the 25.3° (2θ) for anatase (1 0 1), with no significant 27.5° (2θ) for appearance of rutile (1 1 0) [16]. Nishimoto et al. [17] reported that the anatase TiO_2 performed a more prominent photoactivity than the rutile TiO_2. Using the zinc oxide spiking method, it was estimated that the weight of anatase TiO_2 formed on the core kaolin only accounted for approximately 9 wt% of total TiO_2–K particles. Further verification of the nanocrystal size was calculated base on the Scherrer equation, and was found to be consistent with those obtained from TEM of approximately 7.6 nm in diameter.

Subsequent UV–vis diffuse reflectance was performed on the TiO_2–K particles, in order to determine its light absorption capability. A strong shift in the light absorption degree in relative to the

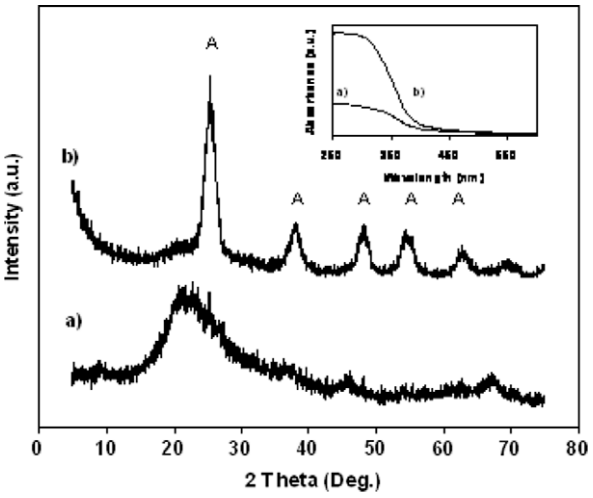

Fig. 5. X-ray diffraction (XRD) and UV–vis diffuse-reflectance spectra of (a) TiO_2–K and (b) bared kaolin. A: Anatase.

bare kaolin was apparently observed at wavelengths lower than 400 nm. This indicated the photo-reaction using the layered TiO_2 nanocrystals can take place using a light source in the UV region. It was observed, however, that the tail of the absorption spectrum at longer wavelengths of the samples may be attributed to the presence of large TiO_2 nanocrystals at the edges of clay platelets [18].

3.3. Variation in the physicochemical properties of TiO_2–K catalysts during repetitive thermal regeneration

In a water treatment system, the photocatalyst particles are usually subjected to hydrodynamic and operating conditions in the semiconductor system, resulting in a possible change of their physicochemical properties. These changes might affect significantly on the photoactivity of the catalysts. Although immobilisation of TiO_2, on separable catalyst support was reported in a number of studies, to date, no study has been found to investigate the possible changes of the physicochemical properties of the photocatalysts under a thermal regeneration. In our study, the TiO_2–K catalysts were recovered and regenerated by a thermo-treatment due to its rapid and simple operation. It is anticipated that the irreversible bound contaminants on the catalyst surface would be easily removed from the particles during the heat treatment. To amplify this hypothesis, the desorption studies were investigated by the cycle washes of spent catalysts in aqueous solution until the dye concentration was constant. It was found that the irreversible bound contaminant was accounted for approximate 2–5% of the total dye which was added before the degradation. Also, it was expected that the repetitive heat treatment can also promote the decomposition of small contaminant molecules attached subterraneous inside the micropores, and result in more available active sites.

In this present study, we investigated the change in the physicochemical properties of the TiO_2–K particles which were experienced a recycling and regeneration cycle at 550 °C for 0.5 h. The impact of thermal regeneration cycles on the photoactivity of the catalysts was evaluated by the CR photodegradation experiments.

Table 1 shows the variation in physicochemical properties of the TiO_2–K particles associated with the number of regeneration cycles. The specific surface area of the catalysts decreased slightly after each thermal regeneration cycled. This might be that the thermal treatment may result in partial collapse of the structural bonding within the layered TiO_2 nanocrystal, therefore, leading to its densification (i.e. decrease in internal pore size). Imai et al. [19] observed that such densification in deposited layered TiO_2 might also be induced by the UV irradiation during photocatalysis. Irradiation with photons which have higher energy than the band gap can induce the densification through the bond cleavage via electronic excitation from the TiO_2 valence band to the conduction band [19].

Another postulation for the decline in specific surface area of the catalysts after repetitive reuse may be due to possible regrowth of the TiO_2 nanocrystals during the thermal regeneration treatment. This postulation was evidenced from the XRD measurement (Fig. 6). Whilst the number of regeneration cycle increases, the intensities of the diffraction peak for the anatase (1 0 1) at 2θ equal to 25.3° increased with intensely narrower peak signals. Such incident may be explained by possible aggregation of the TiO_2 nanocrystals during the course of regeneration. This was proven by the increase in the average TiO_2 nanocrystal size. From Table 1 and Fig. 6, we found that the average nanocrystal size increased from 7.6 nm to 10.1 nm after six regeneration cycles.

Table 1
The characteristic of the recycled titania impregnated kaolin photocatalysts after thermal treatment.

Recycled catalyst	BET specific surface area ($m^2\ g^{-1}$)	Particle diameter (nm)	Pore diameter (nm)
1st	57.66	7.63	8.31
2nd	54.90	8.27	8.62
3rd	52.65	8.71	8.84
4th	49.65	9.38	9.03
5th	47.93	9.72	9.17
6th	44.98	10.13	9.80

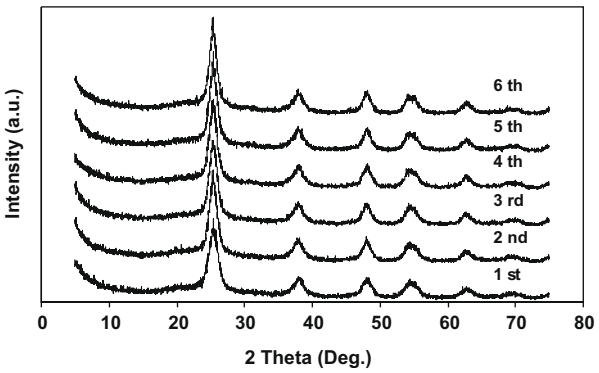

Fig. 6. X-ray diffraction (XRD) of recycled TiO_2–K photocatalysts after cycles of thermal treatment.

One of the prominent findings as indicated by the XRD measurements is that the studied thermal regeneration conditions did not significantly alter the stability of the TiO_2 nanocrystals. Beydoun and Amal [20] reported that the transformation from the anatase to rutile resulted in significant rupture of the Ti–O bonds. We found that, however, after six thermal regeneration cycles, the layered TiO_2 nanocrystals on the kaolin remained in anatase TiO_2 forms. This finding shows that our previous postulation on the nanocrystal re-growth is valid, where the decline in specific surface area is not owed to the photoactive phase transformation. The stability in the layered TiO_2 nanocrystal structure can be related to the formation of Ti–O–Si bonds between the TiO_2 network and siliceous side of kaolin particles during the course of synthesis. It was also known that the presence of Ti–O–Si bonds could suppress the TiO_2 phase transformation from anatase to rutile, and thus directly influenced its stability [20,21]. We used SEM imaging to further confirm the stability of the attached layered TiO_2 on the kaolin surface. Fig. 7 shows that the porous structure of the regenerated catalysts remains with the TiO_2 nanocrystals distributed consistently on the kaolin surface. In overall, we only found that a slight increase in TiO_2 nanocrystal size and its pore diameter is a direct result of the thermal regeneration. No remarkable change on surface morphology was observed after each regeneration cycle.

3.4. Photodegradation of Congo red using TiO_2–K catalysts

Here, we investigated the photocatalytic performances of the TiO_2–K catalysts prepared by treated kaolin clay and the TiO_2–K catalysts regenerated by thermal regeneration cycles. Commercial Degussa P25 TiO_2, which has been commonly used in the many studies, was tested to compare the photodegradation ability with the TiO_2–K photocatalysts.

The photoactivity of the TiO_2–K was tested against 57.4 μmol L^{-1} CR. Control experiments were carried out in the CR solution with UV irradiation and no TiO_2–K. Only 6% CR removal was found in the control experiment under UV irradiation for 7 h. The photoactivity of the TiO_2–K was subsequently tested against bare TiO_2 nanocrystals (i.e. without a kaolin core) and Degussa P25 TiO_2 (Fig. 8). Loading of 10 g L^{-1} of the prepared catalyst and 1 g L^{-1} of P25 were initially applied to attain comparable anatase content. Results showed that the pre-dominant decolourisation of approximately 55% of CR by the TiO_2–K can be achieved after dark adsorption (DA), followed by 70% and 90% CR removal in the first and second hour irradiation. The decolourisation of CR by the P25 TiO_2 was achieved 25% removal during preliminary adsorption, while approximately 80% CR removal can be obtained in 2 h. The rapid CR removal by the TiO_2–K was attributed to the enhanced adsorption of dye molecules on the microporous layered

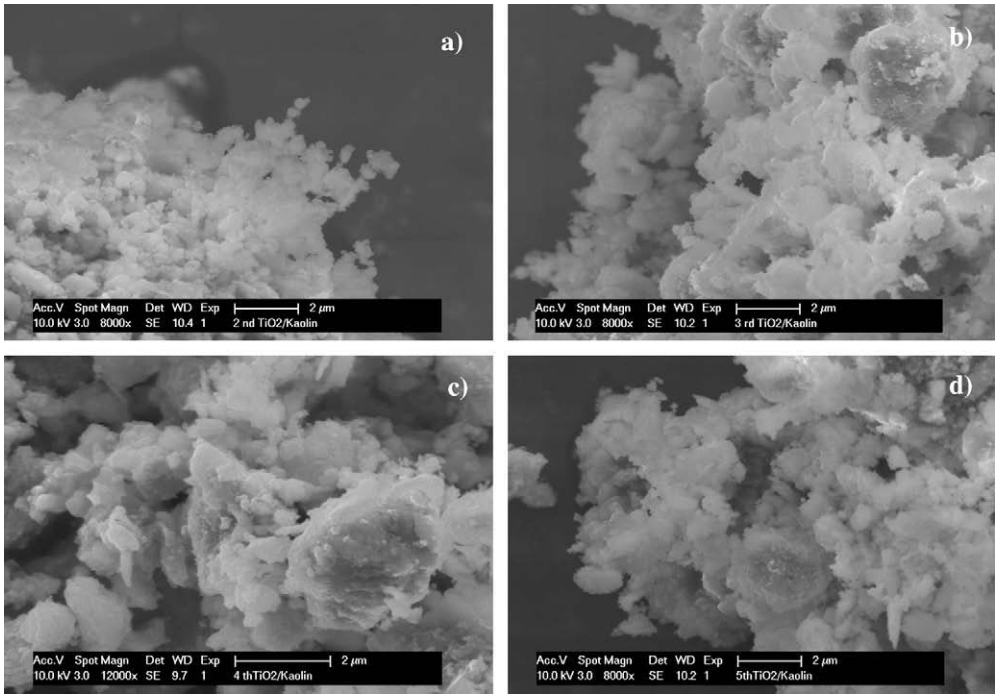

Fig. 7. SEM images of recycled TiO_2–K photocatalyst cycles of thermal treatment (a) 2nd run, (b) 3rd run, (c) 4th run, and (d) 5th run.

TiO_2 nanocrystals, and importantly on the surface of the kaolin particles. Several studies evidenced that the photocatalytic reaction is likely restricted to the adsorbed phase of the catalyst particles [22,23].

The mechanisms of the enhanced photodegradation rate of the TiO_2–K catalysts can be explained that the porous clay support can constantly replenish the CR molecules to the "dynamic equilibrated" surface for surface reaction. When the photoactivity of the TiO_2–K was compared to the P25 TiO_2, it could be observed that both photocatalysts undertake different degradation mechanisms. Titania impregnated kaolin was found to be more adsorption dominant than the P25 TiO_2 and the bare TiO_2 nanocrystals. These can conclude that the rigid porous structure of the kaolin can enhance the adsorption capacity and hence, its photoactivity. Kun et al. [16] proposed that such catalyst improvement via immobilisation might be owed to the force field between the nanocrystal support with particles that inhibit the recombination of electron–hole pairs in the interlamellar clay structure. All these can prove the synergistic effect of core kaolin on its photoactivity, apart as the rigid catalyst support platform.

Photoactivity of the catalysts, however, is known to be highly dependent on its loading in the reaction system [24]. Fig. 9 shows the effects of different photocatalyst loading on the degradation of 57.4 μmol L^{-1} CR. It is expected that the photodegradation rate increases when the catalyst loading varies from 4 to 12 g L^{-1}, as a direct result of more availability of catalyst active sites. In general, the kinetic of photocatalytic degradation is often referred to the Langmuir–Hinshelwood model [3,25]. At a low concentration of the reactant ($C << 1$ mM), this model can be simplified to the apparent first rate order equation [2,26]:

$$\ln\frac{C_0}{C} = kKt = K_{appt} \quad (1)$$

K_{appt} is the apparent first order rate constant (h^{-1}) estimated from the plot of $\ln C_0/C$ versus t (Fig. 9). Table 2 presents the estimated K_{appt} values from the different photocatalyst loadings. Results show

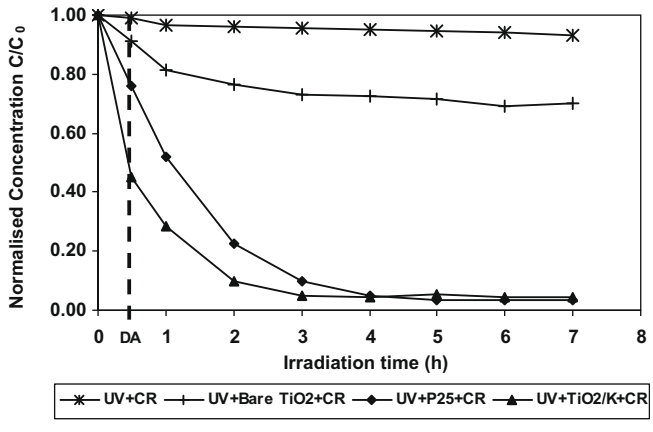

Fig. 8. The photocatalytic degradation of 40 ppm of Congo red by different catalysts.

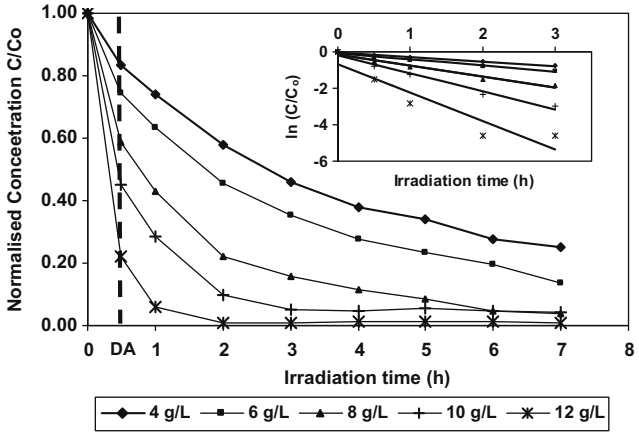

Fig. 9. The photocatalytic degradation of 40 ppm of Congo red by different photocatalyst concentrations.

Table 2
The photocatalytic degradation rate of TiO_2/K at different catalyst concentration.

Catalyst loading ($g\ L^{-1}$)	Photocatalytic degradation rate (K_{appt}) (h^{-1})	R^2
4	0.252	0.9941
6	0.336	0.9802
8	0.607	0.9671
10	0.987	0.9807
12	1.551	0.8734

that the CR degradation kinetic was well-fitted with the apparent first rate order equation model, up to catalysts concentration of 10 $g\ L^{-1}$. The maximum rate of 0.987 h^{-1} was attained at the catalyst concentration of 10 $g\ L^{-1}$. Such fittingness to the kinetic model agreed with the prerequisite adsorption mechanism on the photocatalyst surface prior to surface oxidation reaction.

Estimation in the photoactivity during the repetitive use of the spent photocatalysts was performed to correlate the variation in physicochemical properties of the catalyst with its photoactivity. Fig. 10 shows that the adsorption capacity of the catalysts increases with the thermal regeneration cycles. As stated in earlier sections, such improvements may be well-correlated to the increase in the average pore sizes (i.e. formation of macroporous anatase TiO_2) of the spent catalysts, as evidenced in Table 1. Sasaki et al. [27] proposed that the increase in the number of macropores was associated with the degree of unevenness on the TiO_2 flake surface with the increasing number of thermal regeneration cycle. Similar reaction conditions were tested on the photoactivity of the spent photocatalysts. The K_{appt} values given in Fig. 10 show the competency of the regenerated photocatalysts to the fresh photocatalysts on CR removal in 7 h irradiation. It can be thus, concluded that the TiO_2–K has the potential application in the wastewater treatment owing to its proven economical catalyst lifespan.

3.5. Settleability of the TiO_2–K particles

Since the kaolin particles were made up of the TiO_2–K particle size in the microns range, the feasible application in the slurry semiconductor photoreactor system should be examined. The settleability of particles in a liquid phase is an important physical property in relative to its separation performance. In this study, we examined the settling ability of the TiO_2–K particles by the hindered settling velocity of the photocatalyst particles, which was estimated based on Kynch's theory. Batch settling test was carried out, in which different amount of the photocatalyst (0.05, 0.1, 0.15 and 0.2 g) were simulated with 25 mL of deionised water.

During the analysis, the TiO_2–K particles were allowed to settle under gravitation, in which the decline of particle interface level

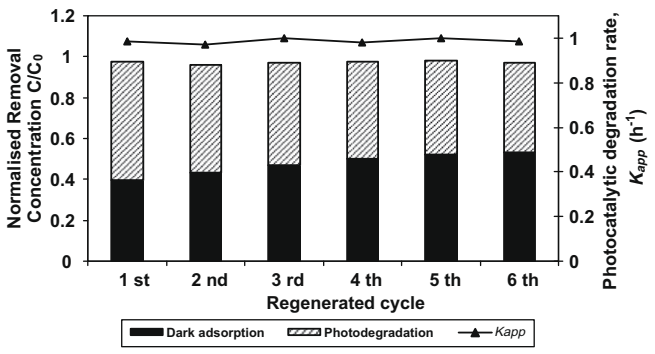

Fig. 10. The photocatalytic degradation performance of recycled TiO_2–K photocatalyst cycles of thermal treatment.

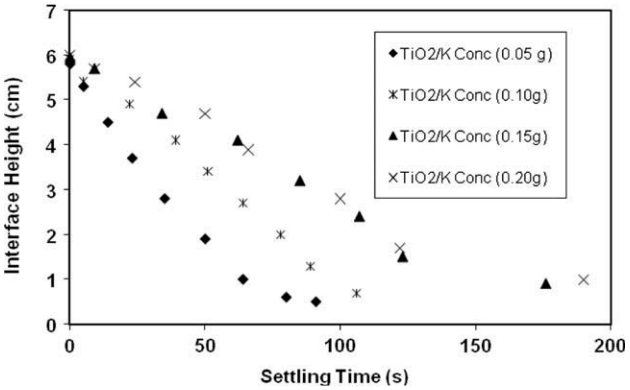

Fig. 11. Settling curves for different TiO_2–K concentration in 25 mL of water.

with time was recorded. The interface height measured at different time intervals for each sample was used to plot the catalyst particle settling curve. The batch settling velocity (v) was estimated from the initial slope of the settling curve. Fig. 11 shows that the batch settling velocity was inversely proportional to the amount of the TiO_2–K particles in suspension. Such a correlation might be attributed to the overall upward flux of the fluid that rises when the settling photocatalyst displaces the water into the sediment zone [28,29]. By fitting the settling kinetics into the linearized Richardson and Zaki correlation (Eq. (2)), the single particle terminal velocity (v_t) was found to be 5.28×10^{-3} m s^{-1}:

$$\log(v_t) = \log(v_{t0}) + (N)\log(1-c) \quad (2)$$

We repeated such batch settling test on the regenerated TiO_2–K particles after each thermal regeneration cycle, and found that the regeneration process did not significantly affect the settling ability of the TiO_2–K particles. It was foreseen that the TiO_2–K catalyst particles performed a higher settling ability than the P25 TiO_2. The high settling ability of the TiO_2–K catalyst makes its application technically promising in a slurry sequential batch reactor system for water/wastewater treatment.

4. Conclusion

The TiO_2 nanocrystals impregnated on the treated kaolin particles were synthesized using the modified two step sol–gel/surface heterocoagulation process. The delaminated flat surface of the treated kaolin prepared under consecutive series of acidification–alkalization-thermal treatment enables homogeneous partition of TiO_2 nanocrystals growth. Furthermore, the chemical interaction between the deposited TiO_2 networks with the siliceous side of the kaolin via Ti–O–Si bonding endorsed the photostability of the prepared photocatalysts. Homogeneous distribution of the TiO_2 nanocrystals on the kaolin surface enhances the photo-oxidation performance of the light photon activation process. During the repetitive thermal regeneration, the surface-deposited microporous anatase TiO_2 was observed to meld into macroporous TiO_2 structure without any significant phase transformation to rutile. These were found to be accompanied by a slight reduction in specific surface area of the catalyst particles and the increase in the average nanocrystal sizes. Parallel photoactivity probing with model CR indicates that the removal efficiency of TiO_2–K was comparable over the six thermal regenerative cycles. Additionally, the TiO_2–K nanocomposites showed a favourable settling ability for separation and recovery of the catalysts in the water treatment system. The high degradation efficiency, physical stability and high settling ability of the TiO_2–K could make the photocatalytic water

treatment technology technically feasible and economically possible for an industrial application.

Acknowledgments

The authors are grateful to the technique advice given by Professor Shaomin Lei from Wuhan University of Technology, China, Associate Professor Huai Yong Zhu from Queensland University of Technology, Australia, for in-kind sample analysis, and Unimin Australia Ltd. for kindly supplying clay mineral. This work was financially supported by the Australian Research Council Linkage Grant (LP0562076) and Australian Water Quality Centre through the Water Environmental Biotechnology Laboratory (WEBL) at the University of Adelaide.

References

[1] U.I. Gaya, A.H. Abdullah, J. Photochem. Photobiol. 9 (2008) 1–12.
[2] I.K. Konstantinou, T.A. Albanis, Appl. Catal., B: Environ. 49 (2004) 1–14.
[3] N.T. Dung, N.V. Khoa, J.-M. Herrmann, Int. J. Photoenergy 7 (2005) 11–15.
[4] O.K. Dalrymple, D.H. Yeh, M.A. Trotz, J. Chem. Technol. Biotechnol. 82 (2007) 121–134.
[5] J.-M. Herrmann, Catal. Today 53 (1999) 115–129.
[6] Y. Gao, H. Liu, Mater. Chem. Phys. 92 (2005) 604–608.
[7] R.K. Wahi, W.W. Yu, Y. Liu, M.L. Mejia, J.C. Falkner, W. Nolte, V.L. Colvin, J. Mol. Catal. A: Chem. 242 (2005) 48–56.
[8] C. Ooka, H. Yoshida, K. Suzuki, T. Hattori, Microporous Mesoporous Mater. 67 (2004) 143–150.
[9] M.N. Chong, V. Vimonses, S. Lei, B. Jin, C. Chow, C. Saint, Microporous Mesoporous Mater. 117 (2009) 233–242.
[10] V. Vimonses, S. Lei, B. Jin, C.W.K. Chow, C. Saint, Appl. Clay Sci. 43 (2009) 465–472.
[11] P. Komadel, J. Madejová, in: F. Bergaya, B.K.G. Theng, G. Lagaly (Eds.), Handbook of Clay Science, Development in Clay Science, vol. 1, Elsevier, The Netherlands, 2006, pp. 263–287.
[12] A. Steudel, L.F. Batenburg, H.R. Fischer, P.G. Weidler, K. Emmerich, Appl. Clay Sci. 44 (2009) 95–104.
[13] D.J.A. Williams, K.P. Williams, J. Colloid Interface Sci. 65 (1978) 79–87.
[14] G. Lagaly, in: F. Bergaya, B.K.G. Theng, G. Lagaly (Eds.), Handbook of Clay Science, Development in Clay Science, vol. 1, Elsevier, The Netherlands, 2006, pp. 141–245.
[15] G. Jozefaciuk, G. Bowanko, Clay Clay Mineral. 50 (2002) 771–783.
[16] R. Kun, K. Mogyorósi, I. Dékány, Appl. Clay Sci. 32 (2006) 99–110.
[17] S.I. Nishimoto, B. Ohtani, H. Kajiwara, T. Kagiya, J. Chem. Soc., Faraday Trans. 181 (1985) 61–68.
[18] H. Yoneyama, S. Haga, S. Yamanaka, J. Phys. Chem. 93 (1989) 4833–4837.
[19] H. Imai, K. Awazu, M. Yasumori, H. Onuki, H. Hirashima, J. Sol–Gel Sci. Technol. 8 (1997) 365–369.
[20] D. Beydoun, R. Amal, Mater. Sci. Eng., B 94 (2002) 71–81.
[21] B.C. Gates, H. Knozinger, Advances in Catalysis, Elsevier Science Book Edition, 2004.
[22] K. Vinodgopal, P.V. Kamat, J. Phys. Chem. 96 (1992) 5053–5059.
[23] K. Kogo, H. Yoneyama, H. Tamaru, J. Phys. Chem. 84 (1980) 1705–1710.
[24] J. Krýsa, M. Keppert, J. Jirkovský, V. Štengl, J. Šubrt, Mater. Chem. Phys. 86 (2004) 333–339.
[25] A. Mills, S. Le Hunte, J. Photochem. Photobiol., A 108 (1997) 1–35.
[26] K. Kabra, R. Chaudhary, R.L. Sawhney, Ind. Eng. Chem. Res. 43 (2004) 7683–7696.
[27] T. Sasaki, S. Nakano, S. Yamauchi, M. Watanabe, Chem. Mater. 9 (1997) 602–608.
[28] R.H. Perry, D.W. Green, Perry's Chemical Engineering Handbook, seventh ed., McGraw-Hill, 1997.
[29] J.F. Richardson, J.H. Harker, J.R. Backhurst, Coulson and Richardso's Chemical Engineering, vol. 2, Particle Technology and Separation Processes, Butterworth–Heinemann, 2003.